J. Fluid Mech. (2001), *vol.* 426, *pp.* 199–228. Printed in the United Kingdom

Droplet deformation in dispersions with unequal viscosities and zero interfacial tension

By ERIC D. WETZEL AND CHARLES L. TUCKER III

Department of Mechanical and Industrial Engineering,
University of Illinois at Urbana-Champaign, Urbana, IL 61801, USA

(Received 4 January 1999 and in revised form 15 June 2000)

An analytical model is presented for the deformation of an ellipsoidal Newtonian droplet, suspended in another Newtonian fluid with different viscosity and zero interfacial tension. The theory is exact for any linear velocity field, and is not limited to small deformations. It encompasses some well-known special cases, such as Jeffery's equation for solid axisymmetric particles and Taylor's small-deformation theory for droplets. Example calculations exhibit droplet stretching, reorientation, and tumbling, and provide a reasonable match to available experimental data on transient and steady droplet shapes. The corresponding rheological theory for dilute dispersions is also derived, in a form that explicitly includes the effects of microstructure on dispersion rheology.

1. Introduction

In this paper we model rheology and microstructure for dispersion in which the two fluids have different viscosities, but interfacial tension is zero. Although interfacial tension usually plays an important role in dispersions, there are many cases where it can be neglected. Examples include the initial stages of polymer blending, where the phases are very viscous and the shear rates are high, and tectonic shearing in the Earth's crust, where the inclusions are very large.

A variety of experiments have demonstrated the general behaviour of droplets with zero interfacial tension. In a steady elongational flow, such droplets extend indefinitely due to the lack of restoring capillary forces (Kalb, Cox & Manley 1981). The rate of extension varies with time, and depends on the ratio of droplet to matrix viscosity. In shearing flows, initially spherical droplets either stretch indefinitely or tumble periodically, again depending on their viscosity ratio (Torza, Cox & Mason 1972). Experimental evidence also suggests that steady shapes may exist in simple shear for droplets with zero interfacial tension. An initially spherical droplet with small interfacial tension and high viscosity ratio will undergo damped tumbling, and eventually reach a steady shape (Torza *et al.* 1972). Taylor (1934) and Rumscheidt & Mason (1961) both found that, once this steady droplet shape is reached, increasing the shear rate does not change the droplet shape. Therefore, this shape may be steady, even in the complete absence of interfacial tension.

Existing analytical models of droplet deformation cannot represent this full range of behaviour observed for systems with zero interfacial tension. One group of models assumes that the droplet shape is a small perturbation from a sphere. This approach was initiated by Taylor (1932), with extensions by Cox (1969), Frankel & Acrivos

(1970), Barthés-Biesel & Acrivos (1973), and Rallison (1980). These theories treat arbitrary viscosity ratios and capillary numbers, but they are accurate only for small deformations. Thus, they are most applicable to systems with high interfacial tension and/or high viscosity ratios. For droplets with zero interfacial tension they apply only to small changes from a spherical shape.

A second group of analytical models, again including interfacial tension, is based on slender-body theory (Taylor 1964; Acrivos & Lo 1978; Khakhar & Ottino 1986). These theories treat highly elongated droplets, but cannot model the transition from a compact to an elongated shape. They also apply only to droplets that are much less viscous than the matrix. In the limit of zero interfacial tension, they predict that the droplet axis elongates at the same rate as the matrix fluid.

In this paper we provide an exact solution for the deformation of a single ellipsoidal Newtonian droplet immersed in a second Newtonian fluid, under conditions of arbitrary viscosity ratio, small Reynolds number, and zero interfacial tension. The solution is exact for all strains, and captures all of the stretching, rotating, oscillating, and steady droplet behaviour observed experimentally. This model can treat general deformation histories, such as a period of extensional flow followed by a simple shear flow, and so is useful for modelling droplet behaviour in complex flows.

Our model is based on the inclusion problem of Eshelby (1957, 1959). Eshelby solved for the strain field in an elastic material with an ellipsoidal elastic inclusion. These results have been widely used to predict elastic moduli, thermal expansion coefficients, and other properties of particle-reinforced composites (e.g. Mura 1982; Taya & Arsenault 1989). Eshelby also suggested that his approach could be used to calculate the creeping flow in and around a droplet in a Newtonian fluid. This extension was first realized by Bilby, Eshelby & Kundu (1975), who presented solutions for an axisymmetric droplet in an axisymmetric stretching flow, and for an elliptic cylinder in a planar elongational flow. This theory has subsequently been applied to other specific flows and droplet shapes, including a three-dimensional ellipsoid in planar elongation (Howard & Brierley 1976) and two-dimensional droplets in planar flow (Bilby & Kolbuszewski 1977). In addition, slender-body theories have been developed for droplets with zero interfacial tension (Spence *et al.* 1988; Wilmott 1989*a*, *b*), and these reproduce the results of the Eshelby theory when the slender droplet is ellipsoidal.

The present work is the first fully three-dimensional treatment of the Eshelby approach for fluids, applicable to general linear flows and droplets of arbitrary ellipsoidal shape and orientation. This implementation is greatly simplified through the introduction of concentration tensors, which are already a standard tool for inclusion problems in elasticity (e.g. Tucker & Liang 1999). Solving the full three-dimensional problem allows us to provide the first comparisons of this theory with experimental droplet measurements, which are typically three-dimensional even in planar flows. We also develop a rheological constitutive equation for a dilute dispersion of identical droplets, and explore its behaviour for simple flows.

It is important to remember that the behaviour of a droplet with *zero* interfacial tension may be very different from a droplet with very *small* interfacial tension. However, our results for zero interfacial tension do provide some insights into small interfacial tension behaviour. We will return to this point in the discussion, after developing the zero interfacial tension theory.

The paper is organized as follows. Section 2 presents the velocity solution within the droplet. We show how this result allows the prediction of droplet shape and orientation for large strains, and leads directly to a rheological theory for a dilute dispersion.

In § 3 we exercise the theory analytically to recover the small deformation theory of Taylor (1934) and the axisymmetric solid particle solution of Jeffery (1922), and we develop relations for steady droplet shapes in simple shear. In § 4 we numerically integrate the model to find droplet shapes and orientations for simple flows, and compare the resulting behaviour with boundary element calculations and published experimental data. We also apply the rheological theory to these flows, demonstrating the dependence of the macroscopic rheology on the microstructure. The paper closes with a brief discussion. The Appendix presents the mathematical details of the theory, including some special relations which simplify its implementation.

2. Theory

2.1. *Problem statement*

Consider a single droplet of one Newtonian fluid suspended in an infinite matrix of another Newtonian fluid. We choose Cartesian coordinates x_i whose origin is fixed at the droplet centroid. For reasonably compact and symmetric shapes each point on the surface of the droplet satisfies

$$G_{ij}x_ix_j + G_{ijkl}x_ix_jx_kx_l + \cdots = 1. \tag{2.1}$$

The time-dependent tensors $G_{ij}, G_{ijkl}, \ldots$, which are symmetric with respect to all pairs of their indices, describe the instantaneous shape of the droplet. We require that the initial shape of the droplet be ellipsoidal, so that

$$G_{ij}x_ix_j = 1 \quad \text{at} \quad t = 0. \tag{2.2}$$

The viscosities of the droplet and matrix may be different, but we assume that interfacial tension is zero. The problem of interest is to impose a uniform velocity gradient $L_{ij} \equiv \partial v_i/\partial x_j$ in the far field,

$$v_i \to L_{ij}x_j \quad \text{as} \quad x_kx_k \to \infty, \tag{2.3}$$

and then calculate $G_{ij}(t), G_{ijkl}(t), \ldots$, the droplet geometry as a function of time. The critical material parameter for this problem is the viscosity ratio $\lambda \equiv \mu^*/\mu$, where μ^* and μ are the viscosities of the droplet and matrix, respectively. Throughout this paper, quantities with a * superscript are associated with the droplet.

Equation (2.3) provides the outer boundary condition for the problem. To complete the formulation, we require that the velocity and surface traction be continuous at the interface between the matrix and droplet. The latter condition implies zero interfacial tension. We also assume that the local Reynolds number for the flow is very small.

The creeping flow assumption allows us to solve for the instantaneous velocity field within the droplet independently of its deformation history. This solution is presented in § 2.2. In § 2.3 we then show how the velocity field within the droplet can be used to model the evolution of the droplet geometry.

2.2. *Droplet velocity field*

For a droplet of arbitrary geometry, the solution of Stokes' equations for our problem results in a complex velocity field within and near the droplet. However, Eshelby (1957, 1959) and Bilby *et al.* (1975) found that assuming an ellipsoidal droplet shape greatly simplifies the problem. While the velocity field around the droplet remains complex, the instantaneous velocity field within inclusion is *linear*:

$$v_i^* = L_{ij}^*x_j. \tag{2.4}$$

This remarkable result, also reported by Goddard & Miller (1967) and implicit in the work of Roscoe (1967), is valid only for ellipsoidal droplets. The droplet velocity gradient L^*_{ij} is, in general, different from the far-field gradient L_{ij}, and depends on the geometry of the ellipsoid and on the viscosity ratio λ.

Eshelby and Bilby *et al.* provide complete solutions for the velocity field both within and around the inclusion. For computing droplet deformations, only the linear velocity field within the inclusion is important. We have found it convenient to re-express the theory in terms of concentration tensors, a practice common to micromechanics (Hill 1963; Benveniste 1987; Tucker & Liang 1999). Using this approach, the inclusion rate-of-deformation tensor E^*_{ij} can be related to the far-field rate-of-deformation tensor E_{ij} by

$$E^*_{ij} = \mathbb{B}_{ijkl} E_{kl}, \tag{2.5}$$

where $E_{ij} \equiv \frac{1}{2}\left(L_{ij} + L_{ji}\right)$. We call $\mathbb{B}_{ijkl}$ the *strain-rate concentration tensor*. Using the results of Bilby *et al.* (1975), the strain-rate concentration tensor can be written as

$$\mathbb{B}_{ijkl} = [\mathbb{I} - (1-\lambda)\,\mathbb{S}]^{-1}_{ijkl}\,. \tag{2.6}$$

The fourth-order identity tensor is defined as

$$\mathbb{I}_{ijkl} = \tfrac{1}{2}(\delta_{ik}\delta_{jl} + \delta_{il}\delta_{jk}). \tag{2.7}$$

$\mathbb{S}_{ijkl}$ is the fourth-order Eshelby tensor (Eshelby 1957), a dimensionless quantity that, for incompressible fluids, depends only on the ellipsoid axis ratios $C \equiv c/a$ and $D \equiv c/b$. Here $a \geqslant b \geqslant c$ are the semi-axis lengths of the ellipsoid. The full analytical Eshelby tensor, when substituted into (2.6) and (2.5), completes the exact solution for E^*_{ij}.

Since the far-field velocity and droplet velocity refer to the same coordinate frame, we expect that any far-field vorticity $\Omega_{ij} \equiv \frac{1}{2}\left(L_{ij} - L_{ji}\right)$ is superimposed onto the droplet flow. However, the velocity solution contains an additional and more subtle result. When the principal axes of the droplet are not aligned with the principal axes of the far-field strain rate E_{ij}, the far-field strain rate also contributes to the droplet vorticity. This effect has been explored for two-dimensional droplets by Bilby & Kolbuszewski (1977). In our notation, the vorticity in the droplet is given by

$$\Omega^*_{ij} = \Omega_{ij} + \mathbb{C}_{ijkl} E_{kl}, \tag{2.8}$$

where Ω^*_{ij} is the inclusion vorticity and we call $\mathbb{C}_{ijkl}$ the *vorticity concentration tensor*. Using the results of Eshelby (1957), this is

$$\mathbb{C}_{ijkl} = (1-\lambda)\mathbb{T}_{ijmn}\,[\mathbb{I} - (1-\lambda)\,\mathbb{S}]^{-1}_{mnkl}\,. \tag{2.9}$$

$\mathbb{T}_{ijkl}$ is the fourth-order alternative Eshelby tensor which, like the Eshelby tensor, is a dimensionless function of ellipsoid axis ratios only and was solved for by Eshelby (1957). The vorticity concentration relation shows that even an irrotational far-field velocity field can induce rotation within the inclusion.

Combining (2.5) and (2.8) provides the inclusion velocity gradient tensor

$$L^*_{ij} = \Omega_{ij} + (\mathbb{B}_{ijkl} + \mathbb{C}_{ijkl})E_{kl}. \tag{2.10}$$

The Appendix provides the analytical formulas for $\mathbb{S}_{ijkl}$, $\mathbb{T}_{ijkl}$, $\mathbb{B}_{ijkl}$, and $\mathbb{C}_{ijkl}$, as well as a convenient procedure for their calculation. Substituting these relations into (2.10) completes the exact solution for the velocity gradient tensor within the inclusion.

2.3. *Microstructural evolution*

2.3.1. *Shape tensor evolution*

Eshelby's solution provides the instantaneous rate of deformation of the droplet. In addition, from basic kinematic arguments we know that an ellipsoid subjected to a linear deformation field always deforms into an ellipsoid, even if the principal deformation axes are not aligned with the principal axes of the ellipsoid (e.g. Cerf 1951). Therefore the requirement of ellipsoidal shape is satisfied for the *deformed* inclusion, and the continuous deformation of the inclusion can be modelled. Thus, Eshelby theory completely and exactly describes the deformation of the ellipsoidal inclusion, and is not limited to small deformations or preferentially oriented flows.

Since the inclusion remains ellipsoidal for all strains, the higher-order terms in (2.1) are exactly zero and the second-order shape tensor $G_{ij}(t)$ completely represents the ellipsoidal droplet geometry at all times. The eigenvalues of G_{ij} are a_i^{-2}, where the a_i are the lengths of the semi-axes of the ellipsoid, so the eigenvalues describe the droplet shape. The eigenvectors of G_{ij} describe the orientation of the principal axes of the droplet relative to the laboratory frame.

To derive an evolution equation for the shape tensor, we take the material derivative of (2.2), apply the chain rule, and utilize the definition of the velocity gradient tensor $\dot{x}_i = L^*_{ij} x_j$. Simplifying yields

$$\dot{G}_{ij} + L^*_{ki} G_{kj} + G_{ik} L^*_{kj} = 0, \tag{2.11}$$

where the dot denotes a material derivative. This equation provides the instantaneous rate of change of the shape tensor in terms of the droplet velocity gradient and the current shape tensor.

The droplet velocity gradient tensor L^*_{ij} is given by (2.10) in terms of the rate-of-deformation and vorticity concentration tensors $\mathbb{B}_{ijkl}$ and $\mathbb{C}_{ijkl}$. These concentration tensors are calculated using the relations in the Appendix and the current semi-axis ratios and rotation tensor. The shape and orientation are determined from the eigenvalues and eigenvectors of the shape tensor, so that (2.10) and (2.11) together form an exact, closed-form equation for the evolution of G_{ij}. We now have a microstructural evolution equation that can be used to predict the deformation and rotation history of a droplet for arbitrary far-field deformation.

2.3.2. *Principal shape tensor and rotation tensor evolution*

For some special problems it is useful to have a separate set of evolution equations for the shape of the ellipsoid and its orientation. To do so we first define *geometric coordinates* y_i. The geometric coordinate system is always aligned with the principal axes of the droplet. Since the droplet will not necessarily be aligned with or steady in the laboratory axes, the geometric coordinate system will not necessarily be aligned with or steady in the laboratory axes. Note that the vorticity of the fluid inside the droplet can differ from the rotation rate of the droplet axes, so the geometric coordinate system is not a co-rotating frame.

We will call the shape tensor in the geometric coordinate system the principal shape tensor G'_{ij}. Points on the droplet surface satisfy

$$G'_{ij} y_i y_j = 1. \tag{2.12}$$

Since the principal shape tensor is always aligned with the principal axes of the

inclusion, it has the property

$$G'_{ij} = \begin{cases} 1/a_i^2 & \text{if} \quad i = j \\ 0 & \text{if} \quad i \neq j, \end{cases} \tag{2.13}$$

where each semi-axis a_i lies along the corresponding y_i coordinate axis. The principal shape tensor is related to the general shape tensor through a rotation tensor R_{ij}, where

$$G_{ij} = R_{iu} R_{jv} G'_{uv}. \tag{2.14}$$

Taking the material derivative of (2.12) and simplifying yields

$$\dot{G}'_{ij} = -L'_{ki} G'_{kj} - G'_{ik} L'_{kj}, \tag{2.15}$$

where L'_{ij} is the velocity gradient tensor within the droplet in the geometric coordinate system, $\dot{y}_i = L'_{ij} y_j$. Substituting (2.13) into (2.15) and simplifying yields the following useful relations:

$$E'_{11} = \frac{\dot{a}_1}{a_1}, \qquad E'_{22} = \frac{\dot{a}_2}{a_2}, \qquad E'_{33} = \frac{\dot{a}_3}{a_3}, \tag{2.16}$$

and

$$E'_{12} = \frac{a_1^2 - a_2^2}{a_1^2 + a_2^2} \Omega'_{12}, \qquad E'_{23} = \frac{a_2^2 - a_3^2}{a_2^2 + a_3^2} \Omega'_{23}, \qquad E'_{31} = \frac{a_3^2 - a_1^2}{a_3^2 + a_1^2} \Omega'_{31}, \tag{2.17}$$

where E'_{ij} and Ω'_{ij} are the rate-of-deformation and vorticity tensors associated with L'_{ij}. These results were also reported by Bilby & Kolbuszewski (1977).

An evolution equation for the rotation tensor R_{ij} can be derived by taking the material derivative of the relationship $x_i = R_{ij} y_j$, and simplifying. The result is

$$\dot{R}_{ij} = \Omega^*_{ik} R_{kj} - R_{ik} \Omega'_{kj}. \tag{2.18}$$

The components of Ω'_{kj}, given in (2.17), can be rewritten in terms of the inclusion rate-of-deformation tensor using $E'_{ij} = R_{ui} R_{vj} E^*_{uv}$. Equations (2.15) and (2.18) can therefore be written explicitly in terms of L^*_{ij} (Wetzel 1999), so that G'_{ij} and R_{ij} could be evolved as microstructural state variables. However, this proves cumbersome for numerical application. Therefore all microstructural evolutions calculated in this paper are performed using the shape tensor G_{ij} and its evolution equation (2.11). G'_{ij} and R_{ij} are only used for finding the steady droplet shape relations in § 3.3.

2.4. *Dispersion rheology*

In dispersions the geometry of the microstructure and the material properties of the two phases determine the macroscopic rheological behaviour. Following Roscoe (1967) and Batchelor (1970), for a dispersion of Newtonian fluids with zero interfacial tension the volume-averaged extra stress $\bar{\tau}_{ij}$ is related to the volume-average rate of deformation $\bar{E}_{ij}$ by

$$\bar{\tau}_{ij} = 2\mu \bar{E}_{ij} + 2\phi(\mu^* - \mu) \bar{E}^*_{ij}, \tag{2.19}$$

where ϕ is the volume fraction of droplets and $\bar{E}^*_{ij}$ is the volume-average rate of deformation within the droplet phase. This constitutive equation is exact for any Newtonian dispersion with zero interfacial tension, regardless of the concentration or geometry of the droplets.

Consider a dilute dispersion composed of droplets with identical shape and orientation, although not necessarily size, and zero interfacial tension. All of the droplets experience the same rate-of-deformation tensor $\bar{E}^*_{ij}$. The droplet rate of deformation

is known as a function of the far-field rate-of-deformation tensor, droplet geometry, and viscosity ratio through (2.5), so the rheological equation for the dispersion is

$$\bar{\tau}_{ij} = 2\mu\bar{E}_{ij} + 2\phi(\mu^* - \mu)\mathbb{B}_{ijkl}\bar{E}_{kl}. \tag{2.20}$$

This constitutive equation is exact within the assumptions of the present theory. Note that $\mathbb{B}_{ijkl}$ is determined by the shape and orientation of the droplets, so this rheological theory explicitly couples the macroscopic rheological behaviour of the mixture to its microstructure. Therefore one must evolve the microstructure through (2.10) and (2.11) in order to use (2.20) to track average stress.

3. Analytical applications

In this section we apply our theory to systems with special geometries, viscosity ratios, and flows. We first use the theory to recover the classic microdynamics results of Jeffery and Taylor. We then predict steady droplet shapes and orientations in simple shear flows. Finally, the rheological theory is used to calculate the effective viscosity of a dilute suspension of spherical inclusions.

All of the derivations in this section require limiting forms of the general tensor relations given in the Appendix. Details of the evaluation of these limits are given by Wetzel (1999).

3.1. *Jeffery's equation*

Jeffery (1922) derived exact equations for the motion of a rigid axisymmetric ellipsoid suspended in a Newtonian fluid undergoing a creeping flow. Since the particle has one axis of symmetry and does not deform, the shape and orientation of the particle are completely described by the axis ratio $C \equiv c/a$ and a unit vector $\hat{\boldsymbol{p}}$. The motion of the particle is described by the rate of change of its direction $\dot{\hat{\boldsymbol{p}}}$. The governing equation for this motion, known as Jeffery's equation, can be written as (Hinch & Leal 1976)

$$\dot{\hat{p}}_i = -\Omega_{ij}\hat{p}_j + \zeta(E_{ij}\hat{p}_j - E_{jk}\hat{p}_j\hat{p}_k\hat{p}_i), \tag{3.1}$$

where ζ is a shape factor which is given by

$$\zeta = \frac{1 - C^2}{1 + C^2}. \tag{3.2}$$

Jeffery's solution is a subclass of our theory, corresponding to an axisymmetric particle with infinite viscosity ratio. For finite axis ratios, the strain-rate concentration tensor $\mathbb{B}_{ijkl}$ (A 13)–(A 19) becomes the zero tensor in the limit of infinite viscosity ratio. This result reflects the fact that a solid finite-sized particle is not deformed by a suspending fluid. In the limit as $D \equiv c/b \to 1$ (axisymmetry) and $\lambda \to \infty$, the vorticity concentration tensor $\mathbb{C}_{ijkl}$ has eight non-zero components (Wetzel 1999):

$$\begin{aligned}\mathbb{C}_{1212} = \mathbb{C}_{1221} = -\mathbb{C}_{2112} = -\mathbb{C}_{2121} \\ = -\mathbb{C}_{3131} = -\mathbb{C}_{3113} = \mathbb{C}_{1313} = \mathbb{C}_{1331} = \frac{1}{2}\frac{1 - C^2}{1 + C^2} = \tfrac{1}{2}\zeta,\end{aligned} \tag{3.3}$$

where the director $\hat{\boldsymbol{p}}$ is oriented along the x_1-axis. We can re-write this vorticity concentration tensor in indicial notation for arbitrary orientation of $\hat{\boldsymbol{p}}$ as

$$\mathbb{C}_{ijkl} = \tfrac{1}{2}\zeta\left(\hat{p}_i\hat{p}_k\delta_{jl} + \hat{p}_i\hat{p}_l\delta_{jk} - \hat{p}_j\hat{p}_l\delta_{ik} - \hat{p}_j\hat{p}_k\delta_{il}\right). \tag{3.4}$$

Using this result directly in (2.8) gives

$$\Omega_{ij}^{*} = \Omega_{ij} + \zeta \left(\hat{p}_i \hat{p}_k E_{jk} - \hat{p}_j \hat{p}_k E_{ik} \right). \tag{3.5}$$

From basic kinematic arguments, the rate of change of $\hat{\boldsymbol{p}}$ can be related to the particle vorticity Ω_{ij}^{*} by (Wetzel 1999)

$$\dot{\hat{p}}_i = -\Omega_{ij}^{*} \hat{p}_j. \tag{3.6}$$

Replacing Ω_{ij}^{*} in this equation with (3.5) and simplifying gives (3.1), and Jeffery's equation is recovered.

Jeffery's equation shows that a slender, rigid ellipsoid in simple shear flow exhibits an undamped, periodic tumbling motion. Given the connection between our theory and Jeffery's equation, it is not surprising that droplets which are much more viscous than the matrix also tumble in simple shear. This behaviour is examined in § 4.3.

3.2. *Taylor small-deformation theory*

Taylor (1934) solved for the velocity field within a spherical droplet suspended in a planar elongational flow, for the case of zero interfacial tension and arbitrary viscosity ratio. This result was generalized by Cox (1969) for any linear flow so that, after some corrections by Frankel & Acrivos (1970), the rate-of-deformation tensor in the droplet can be written as

$$E_{ij}^{*} = \frac{5}{2\lambda + 3} E_{ij}. \tag{3.7}$$

This relation is exact for spherical droplets with zero interfacial tension and arbitrary viscosity ratio.

This velocity solution can also be recovered using our theory. The strain-rate concentration tensor for a spherical droplet can be found by taking the limit of the analytical relations from the Appendix as $C = D \to 1$, yielding

$$\mathbb{B}_{mn} = \begin{bmatrix} \frac{1+4\lambda}{\lambda(3+2\lambda)} & \frac{1-\lambda}{\lambda(3+2\lambda)} & \frac{1-\lambda}{\lambda(3+2\lambda)} & 0 & 0 & 0 \\ \frac{1-\lambda}{\lambda(3+2\lambda)} & \frac{1+4\lambda}{\lambda(3+2\lambda)} & \frac{1-\lambda}{\lambda(3+2\lambda)} & 0 & 0 & 0 \\ \frac{1-\lambda}{\lambda(3+2\lambda)} & \frac{1-\lambda}{\lambda(3+2\lambda)} & \frac{1+4\lambda}{\lambda(3+2\lambda)} & 0 & 0 & 0 \\ 0 & 0 & 0 & \frac{1}{2}\frac{5}{3+2\lambda} & 0 & 0 \\ 0 & 0 & 0 & 0 & \frac{1}{2}\frac{5}{3+2\lambda} & 0 \\ 0 & 0 & 0 & 0 & 0 & \frac{1}{2}\frac{5}{3+2\lambda} \end{bmatrix}, \tag{3.8}$$

where the result is given in the contracted notation defined in table 1 in the Appendix. Substituting this result into (2.5) recovers the small-deformation solution, (3.7).

3.3. *Steady droplet shapes in simple shear*

We now use the theory to derive sufficient conditions under which a three-dimensional drop with zero interfacial tension will have a steady shape in a simple shear flow. In this state, fluid within the droplet deforms, but the streamlines, droplet shape, and droplet orientation remain steady. Note that these droplet shapes are steady only over the time scale on which a zero interfacial tension theory is valid; the presence of even a very small interfacial tension introduces an additional time scale over which interfacial tension effects will eventually be felt. This point is discussed in more detail in § 5.1.

The first theory predicting steady droplet shapes in simple shear was developed by

Taylor (1934). While all of Taylor's experiments had interfacial tension, he observed that droplets with a high viscosity ratio achieved steady shapes that became independent of shear rate at high shear rates. The fact that these shapes are independent of shear rate implies that interfacial tension is not required to maintain them, once they have been achieved. Taylor used a small-deformation theory, neglected interfacial tension, and solved for steady shapes in simple shear. Taylor's result (as corrected by Rumscheidt & Mason 1961) is that that the steady droplet shape satisfies

$$\mathfrak{D} = \frac{5}{2(2\lambda + 3)}. \tag{3.9}$$

Here $\mathfrak{D}$ is the Taylor deformation parameter,

$$\mathfrak{D} \equiv \frac{a_1 - a_2}{a_1 + a_2}, \tag{3.10}$$

and a_1 and a_2 are the long and short axes observed in the plane of motion. This result should be most accurate for very high viscosity ratios, where the deformation is small.

Bilby & Kolbuszewski (1977) used Eshelby theory to solve exactly for the shapes of two-dimensional elliptical droplets in simple shear, finding that the shape is steady if

$$\mathfrak{D} = \frac{1}{\lambda - 1}. \tag{3.11}$$

Roscoe (1967) derived conditions for the steady shape of three-dimensional viscoelastic droplets with zero interfacial tension in a Newtonian matrix, but focused on the implications for suspension rheology rather than on droplet shapes.

The conditions for steady shape are most easily derived using results from § 2.3.2, where we represented droplet shape and orientation with the principal shape tensor G'_{ij} and a rotation tensor R_{ij}. For steady droplet orientation, $\dot{R}_{ij} = 0$. If we also choose the laboratory axes to be aligned with the particle axes ($R_{ij} = \delta_{ij}$) then (2.18) reduces to $L'_{ij} = L^*_{ij}$, or $E'_{ij} = E^*_{ij}$ and $\Omega'_{ij} = \Omega^*_{ij}$. Then (2.17) can be rewritten as

$$E^*_{12} = \frac{a_1^2 - a_2^2}{a_1^2 + a_2^2}\Omega^*_{12}, \qquad E^*_{23} = \frac{a_2^2 - a_3^2}{a_2^2 + a_3^2}\Omega^*_{23}, \qquad E^*_{31} = \frac{a_3^2 - a_1^2}{a_3^2 + a_1^2}\Omega^*_{31}. \tag{3.12}$$

These are the conditions for steady droplet orientation. Since the geometric and laboratory axes are aligned, each ellipsoid semi-axis a_i lies along the corresponding x_i laboratory coordinate axis. For steady droplet shape $\dot{a}_i = 0$, and (2.16) reduce to

$$E^*_{11} = E^*_{22} = E^*_{33} = 0, \tag{3.13}$$

where we still require the laboratory axes to be aligned with the particle axes.

Since we have chosen our laboratory axes to be aligned with the particle axes, the only non-zero components of the strain-rate concentration tensor are given by (A 13)–(A 19). Equation (3.13) then holds if the diagonal components of the applied rate-of-deformation tensor are all zero. This condition is met by a simple shear flow which is oriented such that

$$L_{ij} = \begin{bmatrix} 0 & G & 0 \\ 0 & 0 & 0 \\ 0 & 0 & 0 \end{bmatrix}. \tag{3.14}$$

This result shows that a steady droplet shape in simple shear can occur if the droplet

axes are aligned with the flow axes, which agrees with experimental observations for drops with small interfacial tension.

For this flow the only non-zero inclusion vorticity is $\Omega^*_{12} = -\Omega^*_{21}$, so for steady droplet orientation the only component of (3.12) not satisfied trivially is

$$E^*_{12} = \frac{a_1^2 - a_2^2}{a_1^2 + a_2^2}\Omega^*_{12}. \tag{3.15}$$

Since the particle axes are aligned with the laboratory axes, (2.5) and (2.8) give $E^*_{12} = \mathbb{B}_{1212}G$ and $\Omega^*_{12} = (\frac{1}{2} + \mathbb{C}_{1212})G$. Substituting these results into (3.15) and then using the relations of §§ A.1 and A.2 to eliminate the concentration tensor components in favour of Eshelby tensor components and viscosity ratio yields

$$(\lambda - 1)\mathbb{S}_{12} = \frac{a_2^2}{a_1^2 - a_2^2}, \tag{3.16}$$

where we now use contracted notation (see table 1) for the Eshelby tensor $\mathbb{S}_{ijkl}$. This condition, expressed in coordinates aligned with the particle axes, must be met for the droplet orientation to remain steady in simple shear flow. This condition is implicit in the work of Roscoe (1967), whose theory is based on the solution of Jeffery (1922) for a rigid ellipsoid in a Newtonian matrix.

From § A.1, the off-diagonal components of the Eshelby tensor are bounded by $\mathbb{S}_{12}, \mathbb{S}_{21}, \mathbb{S}_{23}, \mathbb{S}_{32}, \mathbb{S}_{31}, \mathbb{S}_{13} \geqslant 0$. Assuming that $\lambda > 1$, for (3.16) to be satisfied we need $a_1 > a_2$. This requirements allows three possibilities: $a_1 \geqslant a_3 \geqslant a_2$, $a_1 \geqslant a_2 \geqslant a_3$, and $a_3 \geqslant a_1 \geqslant a_2$. We will only investigate the first two scenarios here, as they are most appropriate for comparison with experimental data. The third encompasses the case of elliptic cylinders in shear flows, and can be used to recover (3.11) (Wetzel 1999). A full investigation of all of the possible droplet geometries can be found in Wetzel (1999).

First consider the case $a_1 \geqslant a_3 \geqslant a_2$. This is the physical situation most likely to result from simple shear of an initially spherical droplet, and therefore is most likely the type of drop observed experimentally. The a_1-axis aligned in the flow direction is longest, and the a_2-axis aligned in the shear direction is the shortest. We will use the convention from the Appendix that the ellipsoid semi-axes of length (a, b, c) are chosen such that $a \geqslant b \geqslant c$. Then in the scenario under consideration $a = a_1$, $b = a_3$, $c = a_2$, and $\mathbb{S}_{12}$ defined in the laboratory axes corresponds to $\mathbb{S}_{ac}$ in the material axis system. Equation (3.16) becomes, in the material coordinates and using our axis ratio definitions,

$$(\lambda - 1)\mathbb{S}_{ac} = \frac{C^2}{1 - C^2}. \tag{3.17}$$

Substituting the full form of $\mathbb{S}_{ac} = 1 - \mathbb{S}_{bc} - \mathbb{S}_{cc}$ from § A.1 yields

$$\frac{1}{\lambda - 1} = \frac{D(2C^2 - D^2 - C^2D^2)E(\theta, p) - C^2D(1 - D^2)F(\theta, p) + (D^2 - C^2)(1 - C^2)^{1/2}}{(D^2 - C^2)(1 - D^2)(1 - C^2)^{1/2}}, \tag{3.18}$$

where p and θ are defined by (A 12). An interesting consequence is that this one equation for steady droplet orientation is a function of the two independent axis ratios C and D. Therefore, for a given viscosity ratio and in the absence of interfacial tension, there are *many* steady droplet shapes. To our knowledge this result has not been reported experimentally, nor has it been suggested theoretically.

To find the steady droplet shape for an axisymmetric rod-like drop, with $a_1 > a_3 = a_2$, we can take the limit of (3.18) as $D \to 1$. The result is

$$\lambda = \frac{6(1-C^2)^{1/2} - 3C^2 \ln \dfrac{1+(1-C^2)^{1/2}}{1-(1-C^2)^{1/2}}}{2(1+2C^2)(1-C^2)^{1/2} - 3C^2 \ln \dfrac{1+(1-C^2)^{1/2}}{1-(1-C^2)^{1/2}}}. \tag{3.19}$$

This is the condition for determining the steady droplet shape as a function of viscosity ratio for a rod-like axisymmetric drop with its long axis aligned along the flow direction. Taking the limit of (3.19) as $C \to 0$ gives a value of $\lambda = 3$. If the viscosity ratio is less than 3, there are no steady rod-like axisymmetric droplet shapes.

It is also possible to have a drop that is as wide as it is long, with $a_1 = a_3$ or $C = D$. Since a_2 is the shortest drop dimension, this case corresponds to a disk whose flat face is oriented normal to the shear direction. Taking the limit of (3.18) as $C \to D$ yields

$$\lambda = \frac{(4-C^2)(1-C^2)^{1/2} - 3C\cos^{-1}(C)}{(2+C^2)(1-C^2)^{1/2} - 3C\cos^{-1}(C)}. \tag{3.20}$$

This is the condition for determining the steady droplet shape as a function of viscosity ratio for a disk-like axisymmetric drop with its short axis aligned in the shear direction. Taking the limit of (3.20) as $C \to 0$ gives a value of $\lambda = 2$. If the viscosity ratio is less than 2, there are no steady disk-like axisymmetric droplet shapes.

In a similar manner, the condition for steady droplet shapes for the case of $a_1 \geqslant a_2 \geqslant a_3$ is found to be (Wetzel 1999)

$$\frac{1}{\lambda - 1} = \frac{D(C^2 + D^2 - 2C^2D^2)E(\theta, p) - 2C^2D(1-D^2)F(\theta, p) - D^2(D^2 - C^2)(1-C^2)^{1/2}}{(D^2 - C^2)(1-D^2)(1-C^2)^{1/2}}. \tag{3.21}$$

This configuration is similar to the case immediately above, except that now the shortest droplet axis is oriented along the vorticity axis. In the limit where $a_1 = a_2 > a_3$ the droplet becomes disk-like and axisymmetric, with the shortest axis perpendicular to the shear plane. In this limit, as $D \to C$ in (3.21), we find the solution $\lambda \to \infty$. Therefore this droplet configuration is only steady for solid inclusions.

While we have shown that a variety of steady shapes are possible in simple shear, we have not yet shown that these shapes are stable, or how they might be achieved. These points are explored in § 4.3.

3.4. *Effective viscosity of a dispersion of spherical droplets*

As a check on our rheological theory, we calculate the effective viscosity of a dilute dispersion of spherical droplets. Substituting the spherical droplet rate-of-deformation tensor from (3.7) into the rheological constitutive equation (2.20) and simplifying yields

$$\mu_{\text{eff}} = \mu\left(1 + \phi\frac{5\lambda - 5}{2\lambda + 3}\right), \tag{3.22}$$

where $\mu_{\text{eff}} \equiv \bar{\tau}_{12}/\bar{E}_{12}$. This relation agrees with the result derived by Mellema & Willemse (1983). Since the drops will deform to non-spherical shapes at finite strains, this effective viscosity is only valid at the instant when shearing begins. The subsequent rheological behaviour is examined in § 4.5.

Equation (3.22) can be compared with the well-known result of Taylor (1932),

$$\mu_{\text{eff}} = \mu\left(1 + \phi\frac{5\lambda + 2}{2\lambda + 2}\right), \tag{3.23}$$

which gives the effective viscosity of a suspension with large interfacial tension such that the droplets remain nearly spherical. For equal volume fractions and viscosity ratios, the Taylor viscosity is always higher than the viscosity of the dispersion without interfacial tension.

4. Numerical applications

In this section we present numerical results that explore various types of behaviour of the theory. All computations utilize the shape tensor evolution equation (2.11). The concentration tensors $\mathbb{B}_{ijkl}$ and $\mathbb{C}_{ijkl}$ are computed using the analytical relations of the Appendix, and these concentration tensors are used to calculate the inclusion velocity gradient tensor by (2.10). Results for droplet shape and orientation are expressed in terms of axis ratios and orientation angles, which are calculated from the eigenvalues and eigenvectors of G_{ij}.

Equation (2.11) is integrated in time using a double-precision fourth-order Runge–Kutta technique with adaptive step sizing (Press *et al.* 1992). The accuracy tolerances are set to keep numerical errors less than 1×10^{-10}. The elliptic integral functions of (A 9)–(A 11) are evaluated using Carlson's standard elliptic integral functions (Press *et al.* 1992). Limiting forms of the integrals were also derived and implemented for special geometries where the general formulas become indeterminate (Wetzel 1999).

4.1. *Comparison with boundary element computations*

To confirm the validity of our theory and the accuracy of our numerical implementation, we compare our results with direct numerical simulations of single droplets. While there are numerous examples of such calculations in the literature (e.g. Kennedy, Pozrikidis & Skalak 1994; Cristini, Blawzdzieweicz & Loewenberg 1998), there are few published results for droplets with zero interfacial tension. We will compare our results with droplet deformations predicted by M. Toose (1998, personal communication) using a three-dimensional boundary element method. Figure 1(*a*) compares the droplet shape and orientation angle θ calculated from our theory and from the boundary element computations, for simple shear of an initially spherical drop with viscosity ratio $\lambda = 3$. The calculations are carried out to a maximum strain of $Gt = 5.0$, where G is defined in (3.14). θ is the angle between the major axis of the drop and the flow direction, and droplet shape is described by the axis ratios $C = c/a$ and $D = c/b$. Agreement is extremely good, with some differences at higher strains as mesh distortion limits the accuracy of the boundary element code. Figure 1(*b*) compares the results from the two methods for the planar elongational flow defined by (4.3) and a viscosity ratio of $\lambda = 18.6$. Again, agreement between the two methods is excellent.

4.2. *Droplet evolution in uniaxial elongation*

Figure 2 shows the shape evolution of an initially spherical droplet as a function of strain in a uniaxial elongational flow, defined as

$$L_{ij} = \begin{bmatrix} 2U & 0 & 0 \\ 0 & -U & 0 \\ 0 & 0 & -U \end{bmatrix}. \tag{4.1}$$

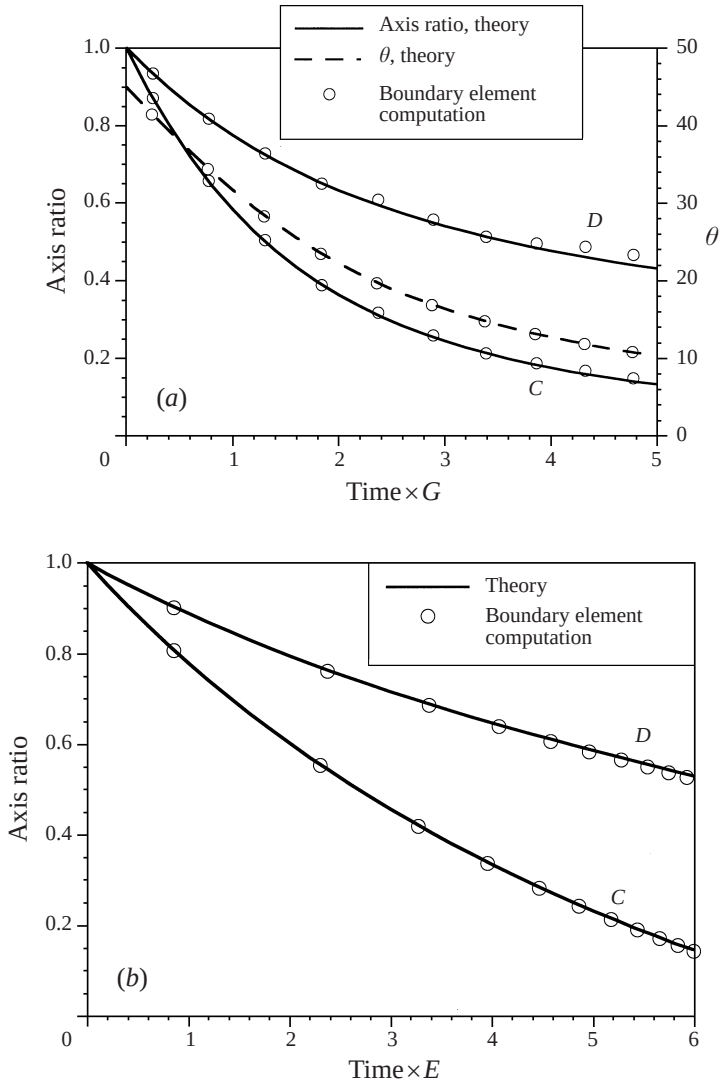

FIGURE 1. Comparison of the theory with boundary element computations by M. Toose. (*a*) Simple shear of an initially spherical droplet with $\lambda = 3$. (*b*) Planar elongation of an initially spherical droplet with $\lambda = 18.6$.

For all viscosity ratios the droplet elongates into a prolate ellipsoid. The deformation of the drop is plotted in terms of the parameter α, defined as

$$\alpha \equiv a/r_o, \tag{4.2}$$

where r_o is the initial droplet radius and a is the length of the long semi-axis of the deformed ellipsoid.

The initial rate of droplet deformation decreases as the viscosity ratio increases, while for $\lambda < 1$ the initial deformation rate is higher than the imposed rate. This latter result has been observed experimentally (Delaby *et al.* 1994).

Once the droplet is elongated it deforms at the applied strain rate regardless of viscosity ratio, and the curves become parallel. This occurs because the external force

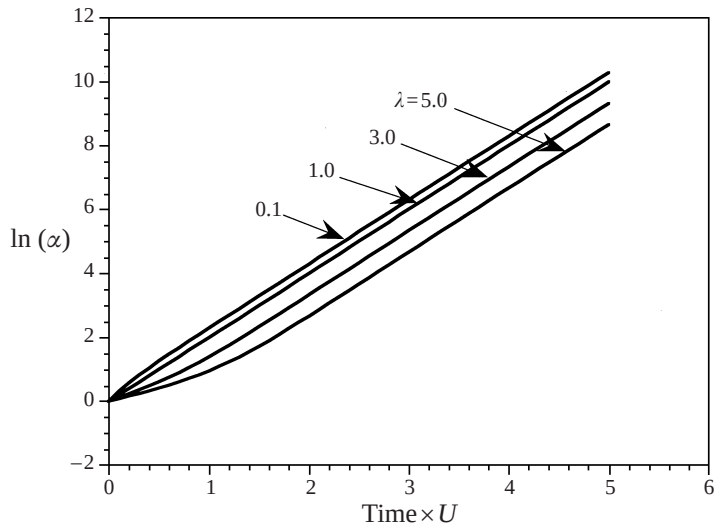

FIGURE 2. Droplet deformation α as a function of strain for initially spherical droplets in uniaxial elongation.

acting on one half of a slender axisymmetric droplet, ignoring numerical factors and logarithmic slender-body factors, equals $\mu(E_{11} - E^*_{11})a^2$, while the internal force at the centre is $\mu^* E^*_{11} b^2$. Equating these two forces gives $\lambda(b/a)^2 = (E_{11}/E^*_{11}) - 1$. Thus, provided that $(a/b)^2$ is large compared to λ, we have $E^*_{11} \approx E_{11}$ and the droplet elongates at nearly the same rate as the external fluid.

4.3. *Droplet evolution in simple shear*

The behaviour of an initially spherical droplet in simple shear flow is shown in figure 3. The flow is defined in (3.14) and θ is the angle between the major axis of the drop and the x_1-axis. The a and c axes lie in the shear (x_1, x_2)-plane and the b-axis is oriented in the vorticity (x_3) direction. Two regimes are apparent: for $\lambda \leqslant 3$ the droplet stretches indefinitely, while for $\lambda \geqslant 5$ the droplet rotates periodically. (The period for $\lambda = 5$ is greater than the maximum plotted strain.)

Figure 3(b) shows the droplet width b during deformation. For viscosity ratios greater than unity the drop decreases in width, while for viscosity ratios less than unity the drop actually increases in width as it is stretched. Similar effects have been observed experimentally in viscoelastic fluids at $\lambda = 0.34$ and 0.13 (Levitt & Macosko 1996), but were attributed to normal stress differences. Our results show that droplet widening can occur in purely Newtonian systems when the viscosity ratio is less than unity. Note that even without interfacial tension, a droplet in a planar flow experiences three-dimensional deformation.

The periodic behaviour shown in figure 3 for high-viscosity, initially spherical droplets represents the transition between two dynamic regimes, tumbling and wobbling. This behaviour was first reported by Bilby & Kolbuszewski (1977), who called the regimes rotation and oscillation. This behaviour can be achieved by starting with non-spherical initial shapes, as shown in figure 4. The initial shapes for this figure are axisymmetric and somewhat elongated in the flow direction ($a > b = c$), and $\lambda = 10$. The axis of the longest droplet (dotted curves) tumbles, executing complete rotations that are reminiscent of the Jeffery orbits of rigid ellipsoids. However, the axis changes length substantially over the period of rotation. The axis of a shorter

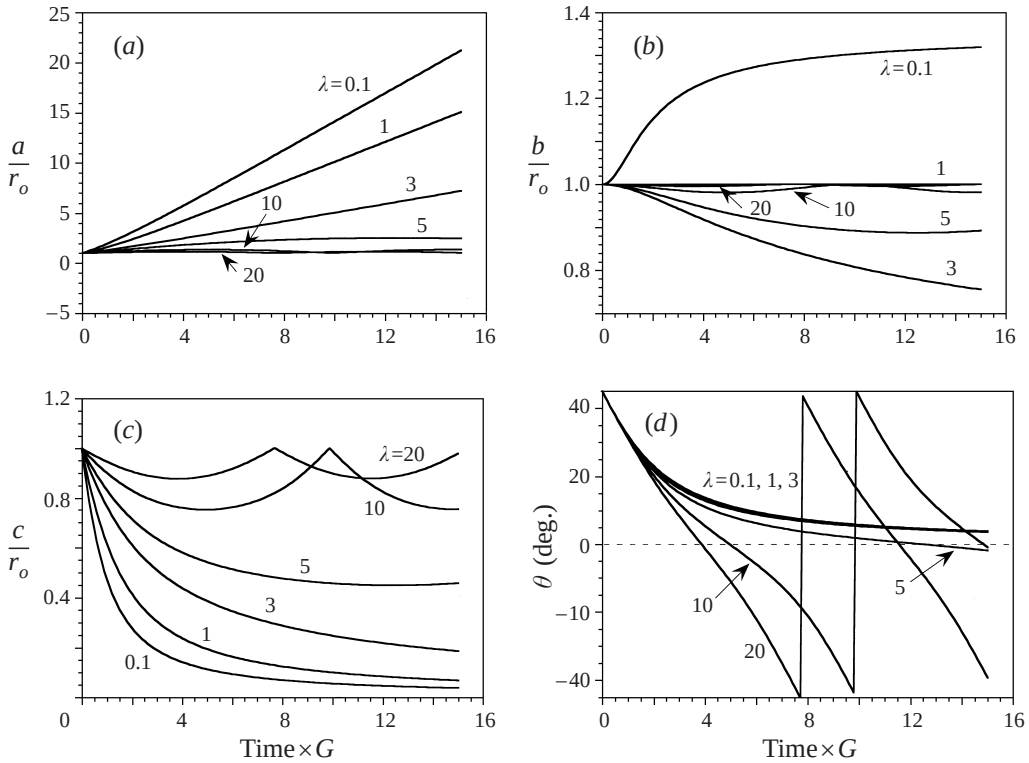

FIGURE 3. Evolution of initially spherical droplets in simple shear. (*a*) Scaled axis length a/r_o. (*b*) Scaled axis length b/r_o. (*c*) Scaled axis length c/r_o. (*d*) Orientation angle of droplet major axis.

droplet (broken curves) wobbles within a narrow range about $\theta = 0$, and the change in the axis length is small. A droplet with intermediate length (solid curves) rotates from $+45^\circ$ to -45°, and is circular in the (x_1, x_2)-plane at these extremes. This is the same transition behaviour as shown by the initially spherical droplet, although this droplet is not spherical when $a = c$.

The dash-dot curves in figure 4 are for an initial shape that is very close to the axisymmetric steady shape given by (3.19). This droplet wobbles with a very small amplitude, changing less than $\pm 1^\circ$ in angle and ± 0.01 in aspect ratio. Although not shown in this figure, droplets whose aspect ratio a/c at $\theta = 0$ is less than this steady value but greater than unity will wobble, while making a/c initially less than unity will lead to tumbling. Bilby & Kolbuszewski (1977) predicted this behaviour for two-dimensional drops, and we see here that three-dimensional drops exhibit the same behaviour.

This variety of behaviour in simple shear flow is a consequence of a competition between vorticity-induced rotation, deformation-induced rotation, and droplet stretching. The vorticity-induced rotation, represented here by the Ω^*_{ij} term in (2.18), rotates the droplet clockwise in this simple shear flow. The vorticity of a reasonably compact droplet is nearly equal to the far-field vorticity. The deformation-induced rotation is represented by the Ω'_{ij} term in (2.18). This mechanism pulls the droplet axis towards the principal stretch direction, $+45^\circ$ in simple shear, and increases in magnitude as the droplet axis deviates from the principal stretch direction. Deformation-induced rotation is most significant for compact droplet shapes, where a small off-axis elon-

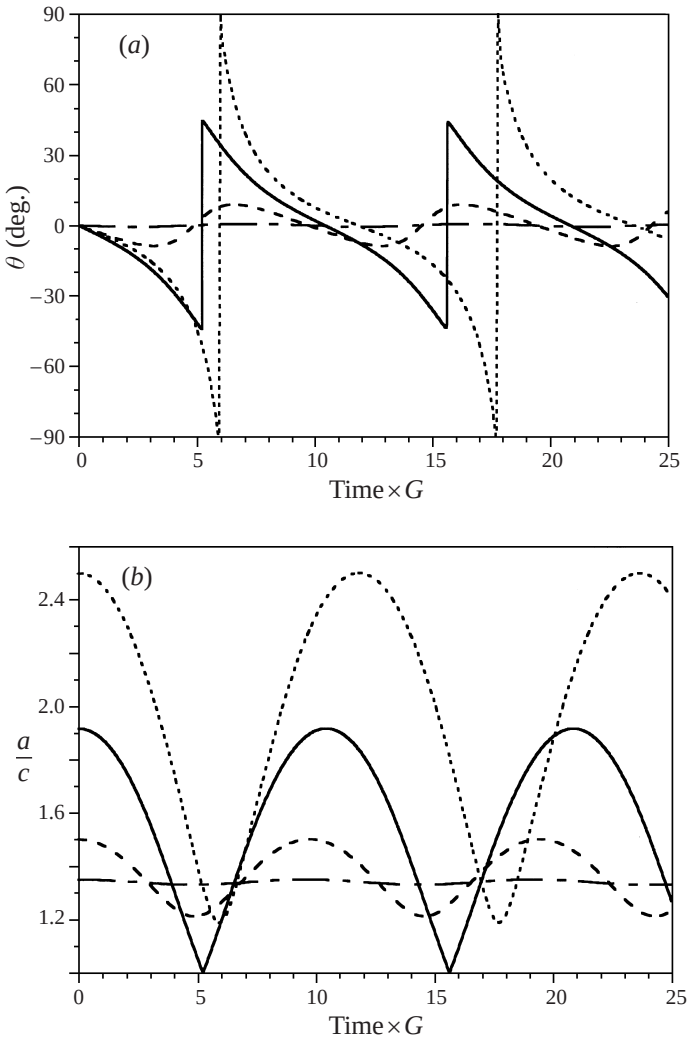

FIGURE 4. Behaviour of initially non-spherical droplets in simple shear for $\lambda = 10$. Initial shapes are axisymmetric with aspect ratios of 2.5 (dotted curves), 1.9177 (solid curves), 1.5 (broken curves), and 1.35 (dash-dot curves). (*a*) Major axis orientation. (*b*) Ratio of axis lengths.

gation can cause a large reorientation of the droplet's principal axis. In addition to these rotations, each principal axis of the droplet stretches at a rate proportional to the far-field stretch rate parallel to that axis. In simple shear this rate is maximum when the axis is oriented at $+45°$, zero at $0°$, minimum at $-45°$, and zero at $\pm 90°$.

The steady droplet shape is oriented at $\theta = 0$, so there is no stretching along the droplet's principal axes. As pointed out by Taylor (1934), for this steady shape the vorticity-induced rotation and the deformation-induced rotation are exactly balanced, and the droplet shape is stationary even though the fluid within the droplet is not. This balance was the basis for the derivation of steady drop shapes in § 3.3.

If a high-viscosity droplet is considerably more elongated than this, like the dotted curves in figure 4, then vorticity-induced rotation dominates and the droplet tumbles.

The rotating droplet sees periodic extension and compression along its main axis, which causes the periodic change in droplet shape.

Now suppose that the droplet is only slightly more elongated when at $\theta = 0$ than the steady shape, like the broken curves in figure 4. Initially vorticity-induced rotation is still dominant and the droplet rotates clockwise, but more slowly than the tumbling drop. Once $\theta < 0$, the long axis of the droplet contracts. This shortened droplet is more sensitive to deformation-induced rotation, causing it to rotate counter-clockwise until $\theta > 0$. In this quadrant the droplet axis stretches, the elongating droplet rotates clockwise, and the cycle begins again.

These wobbling trajectories are orbits around the steady droplet shapes discussed in § 3.3; in the language of dynamical systems they are centres (Bilby & Kolbuszewski 1977). Thus, the steady shapes are neutrally stable: if the droplet is perturbed from its steady shape then it will oscillate in an undamped manner, always remaining close to the steady shape. We have also confirmed that these shape are neutrally stable with respect to small changes in viscosity ratio and far-field flow.

Returning to the initially spherical droplets of figure 3, the same reasoning explains the transition from periodic rotation to stretching. As pointed out by Hinch (1975), an initially spherical droplet with $\lambda \gg 1$ rotates almost with the vorticity of the flow. Owing to its rotation it sees a periodic extension and compression, but due to its high viscosity it experiences little deformation. This is the periodic behaviour seen in figure 3 for $\lambda \geqslant 5$. As λ decreases, deformation-induced rotation increases, and this slows the rotation when the long axis of the droplet is between $\theta = 45^\circ$ and $\theta = 0$. Slower rotation in this orientation range leads to even more stretching, and a runaway process develops in which the droplet stretches without bound as its long axis rotates asymptotically towards the flow direction. This is the stretching regime seen in figure 3 for $\lambda \leqslant 3$.

4.4. *Comparison with experiments*

While there have been many experimental studies of droplets, very few have been conducted with zero interfacial tension. Here we compare our theory to the limited available data.

4.4.1. *Planar elongational flow*

Figure 5 compares our computed drop shapes to those measured experimentally by Kalb *et al.* (1981) for a planar elongation flow,

$$L_{ij} = \begin{bmatrix} E & 0 & 0 \\ 0 & -E & 0 \\ 0 & 0 & 0 \end{bmatrix}. \tag{4.3}$$

The experiments were performed in a four-roll mill using initially spherical drops with negligible interfacial tension and various viscosity ratios. The deformation parameter α is defined in (4.2). Both theory and experiments exhibit identical rates of deformation at small and large strains. At small strains, the experiments and calculations agree with Taylor's small-deformation theory, represented by the solid lines. The equivalence of our theory to Taylor's small deformation result was demonstrated analytically in § 3.2. At large deformations, the rate of droplet extension becomes equal to the applied deformation rate, as discussed in § 4.2.

The general shapes of the experimental and theoretical curves are similar, but for intermediate viscosity ratios the quantitative agreement is not good. Figure 1(*b*) showed that our computations closely match the boundary element calculations for

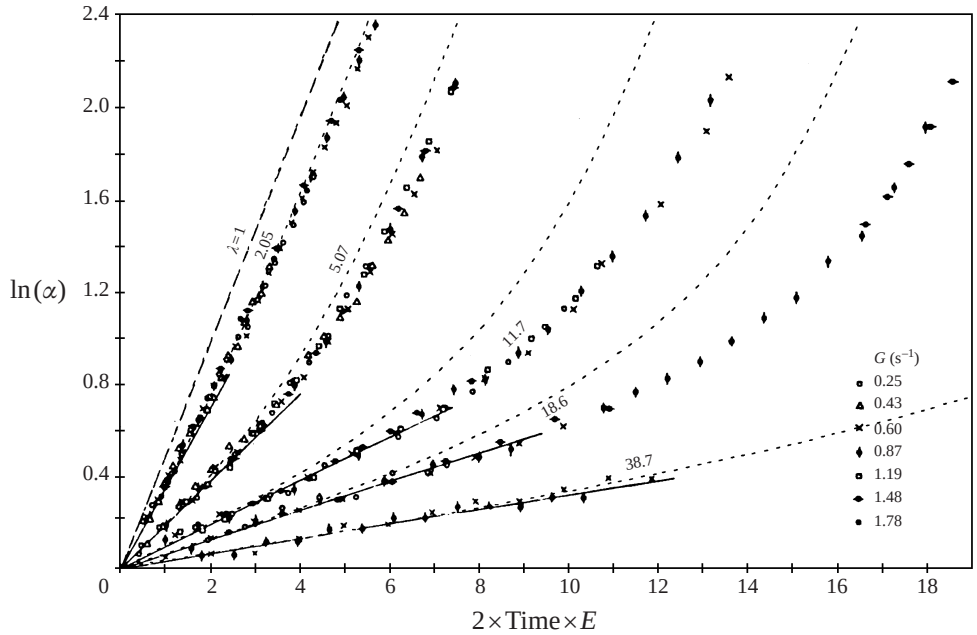

FIGURE 5. Droplet extension in planar elongational flow. Points represent experiments from Kalb *et al.* (1981), dashed curves are the present theory, and solid lines represent Taylor's small-deformation theory (3.7) (reproduced by permission).

this flow and $\lambda = 18.6$. This suggests that our calculations are accurate for these flows. We suspect that the differences in figure 5 are due to non-ideal features of the experiment, such as wall effects, non-uniform extension rate, or a non-spherical initial droplet shape.

4.4.2. *Droplet rotation in simple shear*

Torza *et al.* (1972) reported droplet rotation in simple shear for initially spherical drops with zero interfacial tension and a viscosity ratio of $\lambda = 21$ (their system 28). Figure 6 compares their experimental results with predictions of our theory. Theoretical calculations are shown for an initially spherical drop (initial axis ratio $D_o = 1$). For both the experiment and the calculation the droplet elongates initially along the $+45°$ axis, reaches its maximum elongation with the long axis parallel to the flow, and returns to a sphere along the $-45°$ axis. Only the first cycle measured by Torza *et al.* is plotted, but nearly identical deformation behaviour was observed for a second cycle. This repetition suggests that the droplet evolution is periodic. Torza *et al.* measure a period of oscillation (scaled by the shear rate) of 8.88, while the theory predicts a scaled period of 7.62.

The measured deformations are much greater than the theoretical predictions assuming an initially spherical drop. Torza *et al.* attribute the discrepancy to either diffusion effects or non-idealities of the flow apparatus. Since the droplet was viewed only along the vorticity axis, another source of error could be a non-spherical initial droplet shape. Also shown in figure 6 is the evolution of a droplet that is initially circular in the plane of flow but is a factor of 3.32 thinner in the vorticity direction ($D_o = 0.302$). This deviation from sphericity produces deformations almost identical to those observed by Torza *et al.*, with a predicted period of oscillation of 8.89. Although

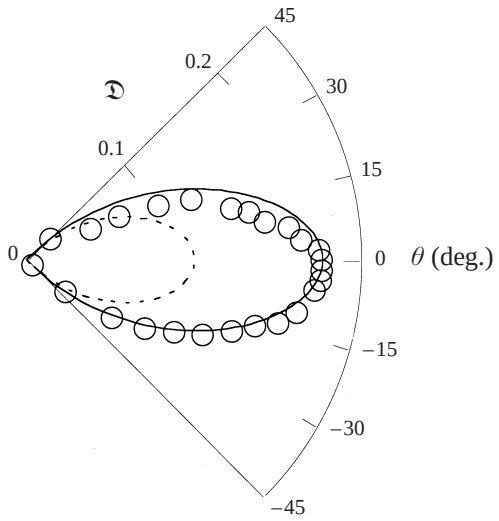

FIGURE 6. Droplet deformation and orientation in simple shear flow. Circles: experimental data from Torza *et al.* (1972); broken line: theory with $D_o = 1$; solid line: theory with $D_o = 0.302$. $\mathfrak{D}$ is defined in (3.10).

it seems unlikely that such significant deviations would have gone unnoticed by the experimenters, it is possible that smaller deviations of this type contributed to the overall experimental error.

4.4.3. *Steady droplet shapes in simple shear*

Taylor (1934), Rumscheidt & Mason (1961), and Torza *et al.* (1972) measured steady droplet shapes for systems with small interfacial tension and high viscosity ratio. In all of these cases the initial droplet shape is approximately spherical, and for large viscosity ratios and high shear rates the final steady shape is ellipsoidal with the long axis aligned in the flow direction. In the experiment of Taylor, the droplet approached its steady shape monotonically with time. Torza *et al.* (1972) observed that droplets with high viscosities and zero interfacial tension rotated indefinitely in simple shear flow, but that small amounts of interfacial tension damped these oscillations so that a steady shape resulted. Rumscheidt & Mason (1961) observed that at low shear rates the steady droplet shape was approached monotonically, but at higher shear rates the droplet executed a damped oscillation.

For all of these experiments the interfacial tension is small but non-zero, as evidenced by the progression of the initially spherical droplet towards a steady droplet shape, rather than the undamped rotation calculated in § 4.3. However, Taylor (1934) theorized that, for cases of sufficiently high viscosity ratio and sufficiently low interfacial tension, this steady shape is independent of interfacial tension. Taylor demonstrated this behaviour experimentally by showing that the steady droplet shape was unaffected by increasing the shear rate. Rumscheidt & Mason (1961) also observed that, for their high viscosity ratio systems, the steady droplet shapes remained constant as shear rate was increased. Most of the experiments of Torza *et al.* (1972) are at shear rates where surface tension is quite significant. However, at high shear rates their system 26 oscillated with only very weak damping, so we can be reasonably confident that the steady droplet shape from this experiment is also unaffected by the presence of a small interfacial tension.

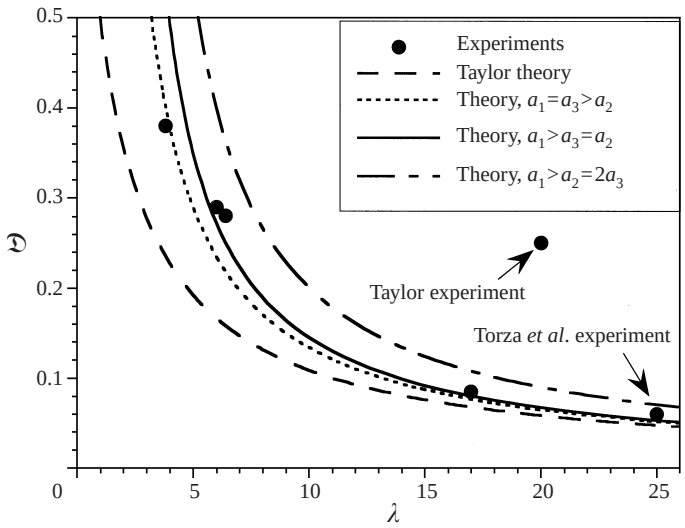

FIGURE 7. Comparison of steady droplet shapes observed in shear flow to theoretical predictions based on the present theory and on Taylor small-deformation theory. All data are from Rumscheidt & Mason (1961) except single points from Taylor (1934) and Torza *et al.* (1972).

Because these experimentally measured shapes are not affected by surface tension, it is interesting to compare them to the steady shapes derived in § 3.3 for zero interfacial tension. One limitation of this comparison is that the experimenters only report a deformation parameter in the shear plane. For the theory of Taylor (1934), the droplet width is assumed to remain constant during shearing (equivalent to requiring $D = C^{1/2}$), so a unique in-plane steady shape is predicted for each viscosity ratio. Our more general analysis predicts a family of possible three-dimensional steady droplet shapes for each viscosity ratio. One shape might be selected from this family during the transient approach to the steady shape. Rather than make assumptions about this transient process, we simply plot steady in-plane droplet shapes for several likely out-of-plane shapes, and see if the experimental results fall within these bounds.

Figure 7 compares the theoretical predictions of § 3.3 with the experimental data of Taylor (1934), Rumscheidt & Mason (1961), and Torza *et al.* (1972) for steady droplet shapes in simple shear. From Torza *et al.* we use only system 26. The data are presented in terms of the Taylor deformation parameter $\mathfrak{D}$, defined in (3.10), where again a_1 and a_2 are the long and short axes in the shear plane. Shown in the figure are our theoretical steady shapes for axisymmetric rod-like drops with the long axis aligned in the flow direction ($a_3 = a_2$), (3.19); axisymmetric disk-like drops with the short axis aligned in the shear direction ($a_3 = a_1$), (3.20); and non-symmetric rod-like drops with the long axis aligned in the flow direction and $a_3 = \frac{1}{2}a_2$, (3.21) with $D = 1/2$. Also shown in the figure are predictions based on the small-deformation theory of Taylor (1934), (3.9).

The results show good agreement between the experimental data and our theory. The data best match the theoretical predictions for droplets with $a_1 > a_3 = a_2$. Except for the single data point from Taylor, the data are bounded by the curves for $a_1 > a_2 = 2a_3$ and $a_1 = a_3 > a_2$. In general, the predictions of our theory match the experimental data much better than Taylor's theory, especially at low viscosity ratios. This behaviour is expected, since Taylor's theory is most accurate at low deformations, but deformations are significant at low viscosity ratios. Comparing

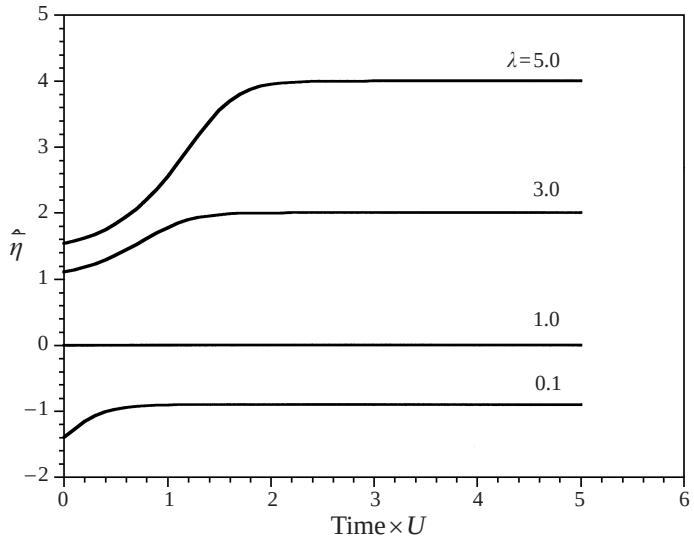

FIGURE 8. Growth of dimensionless elongational viscosity during uniaxial extension of a dilute dispersion with initially spherical droplets.

the $a_2 = 2a_3$ and $a_3 = a_1$ curves also shows that steady droplet shapes are much more sensitive to changes in the droplet's shear-direction dimension than its vorticity-direction dimension.

4.5. *Rheological behaviour*

Using (2.20) we can calculate the macroscopic stress for a dilute dispersion in any homogenous flow. Here we provide stress calculations that complement the droplet shape evolution results of §§ 4.2 and 4.3. Note that droplet shapes must be found as part of this rheological calculation. In all cases the initial dispersion consists of spherical droplets.

Figure 8 shows dimensionless elongational viscosity, defined as

$$\hat{\bar{\eta}} \equiv \frac{(\bar{\tau}_{11} - \bar{\tau}_{22}) - 6\mu U}{6\mu U \phi} = (\lambda - 1)\frac{E^*_{11} - E^*_{22}}{3U}, \tag{4.4}$$

as a function of strain under uniaxial elongation, (4.1). Figure 2 shows droplet elongation during this flow. For all viscosity ratios the mixture undergoes stress growth as the drops deform into cylinders. For $\lambda > 1$, this behaviour is due to the improved reinforcement offered by slender fibre-like droplets as compared to spheres. For $\lambda < 1$, the increase in extensional stress can be attributed to a similar effect, with the higher viscosity matrix becoming more efficiently loaded as the droplets elongate. Note that in all cases the droplets elongate unboundedly, but the extensional viscosity approaches a limiting value. This value corresponds to the effective viscosity of a dispersion in which the droplets extend at the same rate as the matrix, as discussed in § 4.2.

Figure 9 shows the dimensionless shear stress, defined as

$$\hat{\tau}_{12} \equiv \frac{\bar{\tau}_{12} - \mu G}{\mu G \phi} = (\lambda - 1)\frac{2E^*_{12}}{G}, \tag{4.5}$$

as a function of strain for simple shear, (3.14). Figures 3(*a*)–3(*d*) show the droplet

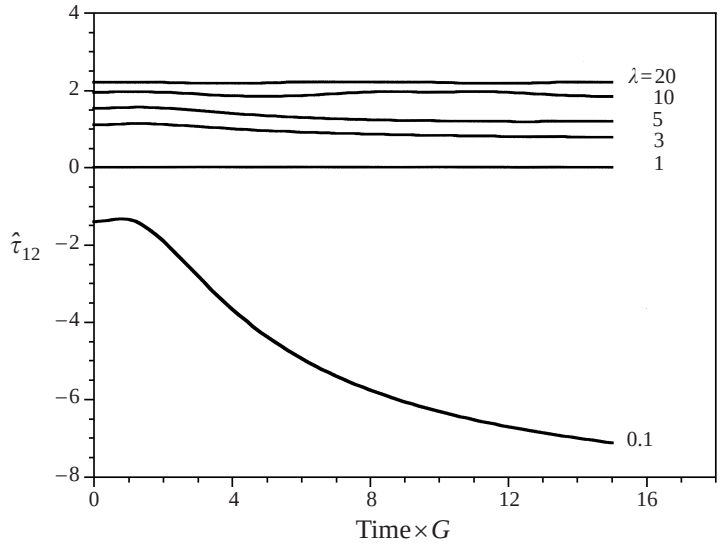

FIGURE 9. Growth of dimensionless shear stress during simple shear of a dilute dispersion of initially spherical droplets.

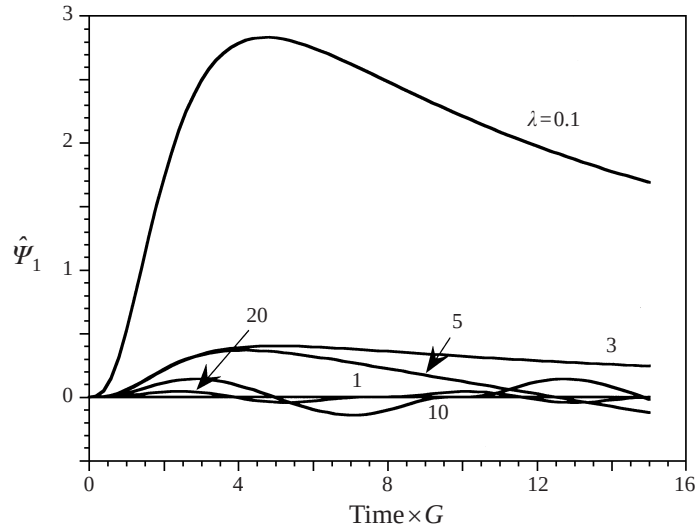

FIGURE 10. Growth of dimensionless first normal stress difference during simple shear of a dilute dispersion of initially spherical droplets.

shape and orientation during this flow. In the stretching regime ($\lambda = 0.1$ and $\lambda = 3$) the shear stress first grows and then decays. The initial growth is due to a reinforcement effect similar to the uniaxial elongational flow case, as the droplets elongate initially at 45° to the flow direction. At higher strains the droplets reinforce less efficiently as they align with the shearing direction, and the stress decreases. For the tumbling regime ($\lambda = 5$, 10 and 20) the shear stress oscillates in phase with the droplet deformation, but the oscillation is small because the droplet shape is never far from spherical.

For this flow figure 10 shows the dimensionless first normal stress difference, defined

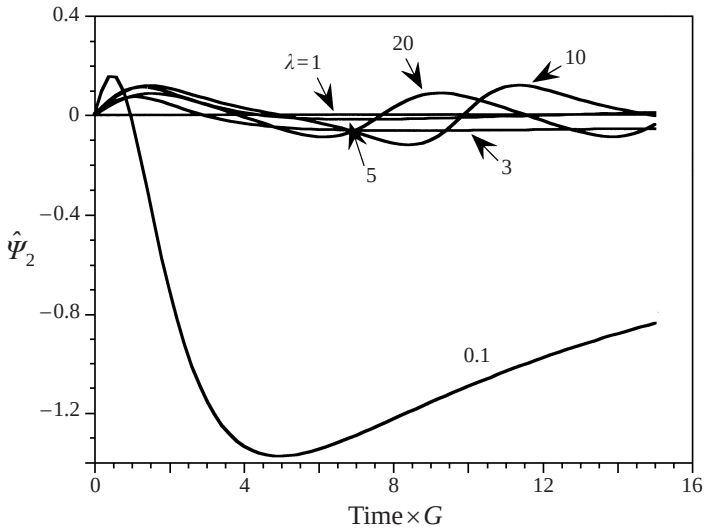

FIGURE 11. Growth of dimensionless second normal stress difference during simple shear of a dilute dispersion of initially spherical droplets.

as

$$\hat{\Psi}_1 \equiv \frac{\bar{\tau}_{11} - \bar{\tau}_{22}}{\mu G \phi} = 2(\lambda - 1)\frac{E^*_{11} - E^*_{22}}{G}. \tag{4.6}$$

For the stretching regime cases ($\lambda = 0.1$ and $\lambda = 3$) the first normal stress difference initially grows and then decays toward zero, again due to the initial off-axis alignment of the drops. For the tumbling cases ($\lambda = 5$, 10 and 20) the normal stress difference oscillates in phase with the droplet deformation. When the droplets are aligned with the laboratory axes, either parallel or perpendicular to the flow direction, the first normal stress difference is zero.

We can also define a dimensionless second normal stress difference in simple shear as

$$\hat{\Psi}_2 \equiv \frac{\bar{\tau}_{22} - \bar{\tau}_{33}}{\mu G \phi} = 2(\lambda - 1)\frac{E^*_{22} - E^*_{33}}{G}. \tag{4.7}$$

The second normal stress difference is shown in figure 11 to depend on microstructure similar to the first normal stress difference.

Note from (4.6) and (4.7) that the normal stress differences $(\bar{\tau}_{11} - \bar{\tau}_{22})$ and $(\bar{\tau}_{22} - \bar{\tau}_{33})$ are proportional to the shear rate G, and not to G^2 as in a viscoelastic fluid. This distinction reflects the fundamentally different mechanisms responsible for normal stress effects in viscoelastic fluids and purely viscous dispersions. In a viscoelastic fluid, normal stress is a second-order effect related to elastic memory. The normal stress differences in figures 10 and 11 for the viscous dispersion are a first-order effect caused by flow-induced anisotropy in the microstructure.

5. Discussion

5.1. *Zero versus small interfacial tension*

Our model system imagines two fluids with different viscosities and zero interfacial tension that are completely immiscible. Any real fluid pair will either have interfacial tension, or will be miscible and will interdiffuse. However, in many cases the time

scales for diffusion and interfacial tension effects are much longer than the time scale for deformation due to external flow. In such cases the real system can behave similarly to the model system, and over some range of time the zero interfacial tension theory can provide accurate predictions of droplet behaviour. For the remainder of the discussion we will assume that diffusion is negligible, and focus on interfacial tension effects.

Consider first a droplet that has been elongated by a far-field flow, which is then stopped. When the far-field flow is halted, a droplet with zero interfacial tension simply maintains its shape. However, a droplet with finite interfacial tension relaxes back to a spherical shape or, if it has been extended enough, breaks up into smaller droplets. Relaxation and breakup occur over a time scales t_r and t_b that are proportional to $\mu a_0/\sigma$, where σ is the interfacial tension and a_0 is the radius of the spherical droplet. These time scales also depend on droplet shape: as droplet aspect ratio increases, the relaxation time t_r increases while the breakup time t_b decreases. Once the far-field flow has stopped, t_r and t_b are the only time scales in the problem. The droplet behaviour is approximated by zero interfacial tension theory only for $t \ll t_r$ and $t \ll t_b$, such that droplet deformation is negligible.

Next, consider the effect of a steady elongational flow on an initially spherical drop. Droplets with zero interfacial tension extend indefinitely, while droplets with finite interfacial tension either reach a steady shape or extend until capillary instabilities cause breakup. We can characterize the flow by its scalar deformation rate E, and define a characteristic time for flow-induced deformation $t_f = 1/E$. At times less than t_r, relaxation effects are unimportant and, if $t_f \ll t_r$, the droplet can experience large deformation before interfacial tension effects become significant. Zero interfacial tension theory can be used to model deformation during this period. As the droplet stretches and its cross-section decreases, t_b also decreases, so that eventually breakup occurs. Zero interfacial tension theory should be applicable to the deformation of a droplet up to this point of capillary instability. Such an approach for modelling the extension and breakup of droplets is philosophically similar to that proposed by Khakhar & Ottino (1987). Khakhar & Ottino treated droplets that were already stretched into a slender shape and had $\lambda \ll 1$. The present theory has the advantage of treating arbitrary viscosity ratios, and can start from a compact droplet shape.

The situation for the startup of simple shear flow is more subtle. First consider droplets with low viscosity ratio, say $\lambda < 3$. With zero interfacial tension such a droplet stretches indefinitely. With finite interfacial tension, the droplet behaves much as it does in elongational flow: if $t_f > t_r$ then the droplet reaches a limiting shape, or breaks into two droplets. However, if $t_f \ll t_r$ then the droplet shape evolution will be very close to zero-tension theory, up until the point where reductions in droplet cross-section lead to breakup.

At higher viscosity ratios, say $\lambda > 5$, an initially spherical droplet rotates periodically in simple shear. With zero interfacial tension this oscillation continues indefinitely, but a small interfacial tension damps the oscillation and brings the droplet to a steady shape. The zero interfacial tension theory also predicts that steady shapes are possible in simple shearing flows, but these can only be realized by starting with the steady shape as an initial condition. The steady shapes for zero interfacial tension and small interfacial tension are, however, related. Experiments and small-deformation theory show that steady droplet shapes derived from damped oscillations, once achieved, do not change significantly as interfacial tension decreases. While the dynamics of achieving the steady shape from an initially spherical droplet rely on interfacial tension, the shape itself is independent of interfacial tension provided the

strain rate is large. This observation is supported by the close agreement in § 4.4.3 between experimentally measured shapes and the steady shapes predicted by the zero interfacial tension theory.

To date, no experiments have shown whether the damped steady droplet shape is determined solely by the viscosity ratio, or whether other factors such as deformation history or interfacial tension also play a role. In the latter scenario, running the experiment at different initial shear rates, or stopping and restarting the experiment, could result in different steady droplet shapes. Any of these droplet shapes, once achieved, could still satisfy zero interfacial tension theory, which predicts multiple steady droplet shapes for each viscosity ratio. Alternatively, a small interfacial tension could select a single steady shape at long times. This question could be explored theoretically by adding a small interfacial effect to the present theory, while retaining the assumption of an ellipsoidal droplet. A model of this type has recently been proposed by Maffettone & Minale (1998), but does not reduce to our result when interfacial tension goes to zero unless the droplet is spherical. This possibility remains as a topic for future investigation.

5.2. *Summary*

We have presented a method for exactly calculating the three-dimensional deformation of an ellipsoidal Newtonian droplet immersed in a Newtonian fluid, when interfacial tension and inertia are negligible and the far-field velocity field is linear. The model uses the classical Eshelby solution for ellipsoidal inclusions, exploring the general three-dimensional problem for the first time. Unlike previous Eshelby solutions, the theory is not limited to small deformations, two-dimensional flows, or particular droplet orientations. The theory predicts a rich variety of behaviour, including stretching, tumbling, wobbling, and steady droplet shapes.

Limiting cases of the model were explored to provide information on the behaviour of microstructures with special geometries or viscosity ratios. These special cases reduce to existing theories for dynamic and rheological behaviour, underscoring the generality of the theory with respect to geometry and viscosity ratio. This connection also provides an important link between the dynamic behaviour of solid particle suspensions and liquid droplet suspensions.

The full three-dimensional dynamic droplet solution, implemented here for the first time, provides insight into phenomena that cannot be explored with existing two-dimensional models. Tumbling, wobbling, stretching, and steady shape regimes were observed during simple shear. Analytical investigation of steady droplet shapes showed that, for a given viscosity ratio, a range of steady droplet shapes is possible, and relationships describing these shapes were presented. Also in simple shear, droplet widening for systems with viscosity ratios less than unity was observed. The full three-dimensional rheology of suspensions during deformation was also directly calculated, revealing behaviour that cannot be predicted with microstructure-independent models.

This theory has many applications. Our own interest is to model microstructure development during mixing processes. After solving for the flow field in an industrial mixing device, one could apply our theory to track the evolution of a droplet shape and orientation throughout the flow. In fact, the numerical methods typical of such complex flow modelling should also allow the implementation of our rheological model, so the microstructure and flow problems could be directly coupled. The ability to predict accurately the microstructure in general mixing flows would enable the design of processes that impart some desired microstructure to the material.

This work also contributes to our understanding of microstructural models for

liquid–liquid mixtures. The Doi & Ohta (1991) model and its extensions attempt to develop equations for microstructural evolution and rheology in liquid–liquid dispersions, using the amount and orientation of the interfacial area as a microstructural state variable. The present model, by providing an exact solution of a significant special case, can shed light on the appropriate forms of such models when the two fluids have different viscosity.

This work was supported in part by the National Science Foundation, Grant No. DMI-981320. Eric Wetzel was supported as a National Science Foundation Graduate Research Fellow. We thank Dr Matthijs Toose of the University of Minnesota for performing the boundary element calculations of figures 1(*a*) and 1(*b*), and Professor John Hinch of Cambridge University for suggesting several of the explanations of droplet behaviour.

Appendix. Eshelby tensors and concentration tensors

Eshelby (1957) provides analytical formulas for calculating the Eshelby tensor in the principal axis system of the droplet. In this section we recast Eshelby's results in terms of elliptic integral functions and some convenient algebraic relations between components. The components of the strain-rate and vorticity concentration tensors are then written explicitly in terms of Eshelby tensor components and viscosity ratio. These relations are used to derive analytical results in § 3, and to enable efficient calculations of microstructure and stress as discussed in § 4.

All results are presented in the principal axes of the ellipsoid. Once the relevant tensors have been computed in the principal axis system, they are rotated to the problem coordinates using standard tensor rotation methods.

A.1. *Simplification of the Eshelby tensors*

The complete Eshelby tensor, in the principal axes and contracted notation (table 1), has the form

$$\mathbb{S}_{mn} = \begin{bmatrix} \mathbb{S}_{11} & \mathbb{S}_{12} & \mathbb{S}_{13} & 0 & 0 & 0 \\ \mathbb{S}_{21} & \mathbb{S}_{22} & \mathbb{S}_{23} & 0 & 0 & 0 \\ \mathbb{S}_{31} & \mathbb{S}_{32} & \mathbb{S}_{33} & 0 & 0 & 0 \\ 0 & 0 & 0 & \mathbb{S}_{44} & 0 & 0 \\ 0 & 0 & 0 & 0 & \mathbb{S}_{55} & 0 \\ 0 & 0 & 0 & 0 & 0 & \mathbb{S}_{66} \end{bmatrix}. \tag{A 1}$$

The alternative Eshelby tensor is symmetric with respect to its last two indices but anti-symmetric with respect to its first two indices. Since standard contracted notation requires index symmetry, we define a quasi-contracted notation in table 1 to represent the contraction of its first pair of indices. In quasi-contracted notation and principal axes, the only non-zero components in the alternative Eshelby tensor are $\mathbb{T}_{44}$, $\mathbb{T}_{55}$, and $\mathbb{T}_{66}$.

The fifteen non-zero components which comprise the Eshelby and alternative Eshelby tensors in the principal axis system can be reduced to five independent components by utilizing the relations

$$\mathbb{S}_{13} = 1 - \mathbb{S}_{23} - \mathbb{S}_{33}, \qquad \mathbb{S}_{66} = \tfrac{1}{2}(\mathbb{S}_{12} + \mathbb{S}_{21}), \qquad \mathbb{T}_{66} = \tfrac{1}{2}(\mathbb{S}_{21} - \mathbb{S}_{12}), \tag{A 2}$$

$$\mathbb{S}_{32} = 1 - \mathbb{S}_{12} - \mathbb{S}_{22}, \qquad \mathbb{S}_{55} = \tfrac{1}{2}(\mathbb{S}_{31} + \mathbb{S}_{13}), \qquad \mathbb{T}_{55} = \tfrac{1}{2}(\mathbb{S}_{13} - \mathbb{S}_{31}), \tag{A 3}$$

$$\mathbb{S}_{21} = 1 - \mathbb{S}_{31} - \mathbb{S}_{11}, \qquad \mathbb{S}_{44} = \tfrac{1}{2}(\mathbb{S}_{23} + \mathbb{S}_{32}), \qquad \mathbb{T}_{44} = \tfrac{1}{2}(\mathbb{S}_{32} - \mathbb{S}_{23}), \tag{A 4}$$

Contracted index	Contracted notation index pair	Quasi-contracted notation index pair
1	(1, 1)	(1, 1)
2	(2, 2)	(2, 2)
3	(3, 3)	(3, 3)
4	(2, 3), (3, 2)	(2, 3), −(3, 2)
5	(3, 1), (1, 3)	(3, 1), −(1, 3)
6	(1, 2), (2, 1)	(1, 2), −(2, 1)

TABLE 1. Contracted and full indices for conventional contracted notation (used for both pairs of indices in $\mathbb{S}_{ijkl}$ and the last pair of indices in $\mathbb{T}_{ijkl}$) and quasi-contracted notation (used for the first pair of indices in $\mathbb{T}_{ijkl}$). As an example of the contracted alternative Eshelby tensor, $\mathbb{T}_{66} = \mathbb{T}_{1212} = \mathbb{T}_{1221} = -\mathbb{T}_{2112}$.

along with

$$\mathbb{S}_{11} + \mathbb{S}_{22} + \mathbb{S}_{33} + 2(\mathbb{S}_{32} + \mathbb{S}_{21} + \mathbb{S}_{13}) = 3. \tag{A 5}$$

These identities, to our knowledge, have not been reported in the literature but provide a major simplification to the computation of the Eshelby tensor. We derived these identities through algebraic trial-and-error, starting from the formulas found in Eshelby (1957). These relationships can be partially deduced based on incompressibility arguments, but the full set seems to result from subtleties of the underlying mathematics.

These relations reduce the two Eshelby tensors to five independent components, but for completeness we choose to present explicit formulas for six components. These components are given exactly as a function of ellipsoid axis ratios by Eshelby (1957), and we write his results in terms of elliptic integral functions as

$$\mathbb{S}_{11} = \mathbb{S}_{aa} = 1 + D^2\frac{J_a - J_b}{D^2 - C^2} + \frac{J_a - J_c}{1 - C^2}, \qquad \mathbb{S}_{23} = \mathbb{S}_{bc} = D^2\frac{J_c - J_b}{1 - D^2}, \tag{A 6}$$

$$\mathbb{S}_{22} = \mathbb{S}_{bb} = 1 + \frac{J_b - J_c}{1 - D^2} + C^2\frac{J_a - J_b}{D^2 - C^2}, \qquad \mathbb{S}_{31} = \mathbb{S}_{ca} = \frac{J_c - J_a}{1 - C^2}, \tag{A 7}$$

$$\mathbb{S}_{33} = \mathbb{S}_{cc} = 1 + C^2\frac{J_a - J_c}{1 - C^2} + D^2\frac{J_b - J_c}{1 - D^2}, \qquad \mathbb{S}_{12} = \mathbb{S}_{ab} = C^2\frac{J_b - J_a}{D^2 - C^2}. \tag{A 8}$$

For uniqueness, here we use the convention that the (1, 2, 3) principal axes are aligned with the (a, b, c) axes of the ellipsoid, where $a \geqslant b \geqslant c$. However, all of the relationships derived earlier in this section, as well as those found in § A.2, hold for any ordering of the principal axes. The J_a type integrals can be expressed as

$$J_a = \frac{C^2 D\,[F(\theta, p) - E(\theta, p)]}{(D^2 - C^2)(1 - C^2)^{1/2}}, \tag{A 9}$$

$$J_b = 1 - J_a - J_c, \tag{A 10}$$

$$J_c = \frac{(1 - C^2)^{1/2} - DE(\theta, p)}{(1 - D^2)(1 - C^2)^{1/2}}, \tag{A 11}$$

where $F(\theta, p)$ and $E(\theta, p)$ are elliptic integrals of the first and second kind, respectively. p and θ are given by

$$p = \frac{1}{D}\left(\frac{D^2 - C^2}{1 - C^2}\right)^{1/2}, \qquad \theta = \cos^{-1}(C). \tag{A 12}$$

A.2. *Calculating concentration tensors from Eshelby tensors*

The strain-rate and vorticity concentration tensors are given as a function of the Eshelby tensor through (2.6) and (2.9). In practice, inversion of fourth-order tensors can be computationally intensive. For this reason we derive algebraic equations for the components of the concentration tensors as a function of λ, $\mathbb{S}_{ijkl}$, and $\mathbb{T}_{ijkl}$. To simplify this procedure, all calculations are done in the principal axes. For numerical implementation the concentration tensors must be subsequently rotated to the laboratory axes.

The strain-rate concentration tensor possesses minor symmetry for its first and second pair of indices, and so it can be expressed in contracted notation. In the principal axes, the non-zero components of the contracted strain-rate concentration tensor can be expressed as

$$\mathbb{B}_{11} = \frac{1 + v(\mathbb{S}_{22} + \mathbb{S}_{33}) + v^2(\mathbb{S}_{22}\mathbb{S}_{33} - \mathbb{S}_{23}\mathbb{S}_{32})}{D_b}, \tag{A 13}$$

$$\mathbb{B}_{22} = \frac{1 + v(\mathbb{S}_{33} + \mathbb{S}_{11}) + v^2(\mathbb{S}_{33}\mathbb{S}_{11} - \mathbb{S}_{31}\mathbb{S}_{13})}{D_b}, \tag{A 14}$$

$$\mathbb{B}_{33} = \frac{1 + v(\mathbb{S}_{11} + \mathbb{S}_{22}) + v^2(\mathbb{S}_{11}\mathbb{S}_{22} - \mathbb{S}_{12}\mathbb{S}_{21})}{D_b}, \tag{A 15}$$

$$\mathbb{B}_{12} = -v\frac{\mathbb{S}_{12} + v(\mathbb{S}_{12}\mathbb{S}_{33} - \mathbb{S}_{13}\mathbb{S}_{32})}{D_b}, \qquad \mathbb{B}_{21} = -v\frac{\mathbb{S}_{21} + v(\mathbb{S}_{21}\mathbb{S}_{33} - \mathbb{S}_{23}\mathbb{S}_{31})}{D_b}, \tag{A 16}$$

$$\mathbb{B}_{23} = -v\frac{\mathbb{S}_{23} + v(\mathbb{S}_{23}\mathbb{S}_{11} - \mathbb{S}_{21}\mathbb{S}_{13})}{D_b}, \qquad \mathbb{B}_{32} = -v\frac{\mathbb{S}_{32} + v(\mathbb{S}_{32}\mathbb{S}_{11} - \mathbb{S}_{31}\mathbb{S}_{12})}{D_b}, \tag{A 17}$$

$$\mathbb{B}_{31} = -v\frac{\mathbb{S}_{31} + v(\mathbb{S}_{31}\mathbb{S}_{22} - \mathbb{S}_{32}\mathbb{S}_{21})}{D_b}, \qquad \mathbb{B}_{13} = -v\frac{\mathbb{S}_{13} + v(\mathbb{S}_{13}\mathbb{S}_{22} - \mathbb{S}_{12}\mathbb{S}_{23})}{D_b}, \tag{A 18}$$

$$\mathbb{B}_{44} = \frac{1}{2 + 4v\mathbb{S}_{44}}, \qquad \mathbb{B}_{55} = \frac{1}{2 + 4v\mathbb{S}_{55}}, \qquad \mathbb{B}_{66} = \frac{1}{2 + 4v\mathbb{S}_{66}}, \tag{A 19}$$

where

$$v = \lambda - 1, \tag{A 20}$$

and

$$\begin{aligned} D_b = {} & 1 + v(\mathbb{S}_{11} + \mathbb{S}_{22} + \mathbb{S}_{33}) \\ & + v^2(\mathbb{S}_{11}\mathbb{S}_{22} + \mathbb{S}_{22}\mathbb{S}_{33} + \mathbb{S}_{33}\mathbb{S}_{11} - \mathbb{S}_{12}\mathbb{S}_{21} - \mathbb{S}_{23}\mathbb{S}_{32} - \mathbb{S}_{31}\mathbb{S}_{13}) \\ & + v^3(\mathbb{S}_{11}\mathbb{S}_{22}\mathbb{S}_{33} + \mathbb{S}_{12}\mathbb{S}_{23}\mathbb{S}_{31} + \mathbb{S}_{21}\mathbb{S}_{32}\mathbb{S}_{13} - \mathbb{S}_{11}\mathbb{S}_{23}\mathbb{S}_{32} - \mathbb{S}_{22}\mathbb{S}_{31}\mathbb{S}_{13} - \mathbb{S}_{33}\mathbb{S}_{12}\mathbb{S}_{21}). \end{aligned} \tag{A 21}$$

The vorticity concentration tensor cannot be expressed in conventional contracted notation because it possesses anti-symmetry with respect to its first pair of indices and symmetry with respect to its second pair of indices. We therefore use quasi-contracted notation for the first two indices and contracted notation for the second pair of indices (table 1). The only non-zero vorticity concentration tensor components in the principal axes are

$$\mathbb{C}_{44} = -v\frac{\mathbb{T}_{44}}{1 + 2v\mathbb{S}_{44}}, \qquad \mathbb{C}_{55} = -v\frac{\mathbb{T}_{55}}{1 + 2v\mathbb{S}_{55}}, \qquad \mathbb{C}_{66} = -v\frac{\mathbb{T}_{66}}{1 + 2v\mathbb{S}_{66}}. \tag{A 22}$$

REFERENCES

Acrivos, A. & Lo, T. S. 1978 Deformation and breakup of a single slender drop in an extensional flow. *J. Fluid Mech.* **86**, 641–672.

Barthés-Biesel, D. & Acrivos, A. 1973 Deformation and burst of a liquid droplet freely suspended in a linear shear field. *J. Fluid Mech.* **61**, 1–21.

Batchelor, G. K. 1970 The stress system in a suspension of force-free particles. *J. Fluid Mech.* **41**, 545–570.

Benveniste, Y. 1987 A new approach to the application of Mori-Tanaka's theory in composite materials. *Mech. Mat.* **6**, 147–157.

Bilby, B. A., Eshelby, J. D. & Kundu, A. K. 1975 The change of shape of a viscous ellipsoidal region embedded in a slowly deforming matrix having a different viscosity. *Tectonophysics* **28**, 265–274.

Bilby, B. A. & Kolbuszewski, M. L. 1977 The finite deformation of an inhomogeneity in two-dimensional slow viscous incompressible flow. *Proc. R. Soc. Lond.* A **355**, 335–353.

Cerf, R. 1951 Recherches theoriques et experimentales sur l'effet Maxwell des solutions de macromolecules deformables. *J. Chim. Physique* **48**, 59–84.

Cox, R. G. 1969 The deformation of a drop in a general time-dependent fluid flow. *J. Fluid Mech.* **37**, 601–623.

Cristini, V., Blawzdzieweicz, J. & Loewenberg, M. 1998 Drop breakup in three-dimensional viscous flows. *Phys. Fluids* **10**, 1781–1783.

Delaby, I., Ernst, B., Germain, Y. & Muller, R. 1994 Droplet deformation in polymer blends during uniaxial elongational flow: Influence of viscosity ratio for large capillary numbers. *J. Rheol.* **38**, 1705–1720.

Doi, M. & Ohta, T. 1991 Dynamics and rheology of complex interfaces I. *J. Chem. Phys.* **95**, 1242–1248.

Eshelby, J. D. 1957 The determination of the elastic field of an ellipsoidal inclusion, and related problems. *Proc. R. Soc. Lond.* A **241**, 376–396.

Eshelby, J. D. 1959 The elastic field outside an ellipsoidal inclusion. *Proc. R. Soc. Lond.* A **252**, 561–569.

Frankel, N. A. & Acrivos, A. 1970 The constitutive equation for a dilute emulsion. *J. Fluid Mech.* **44**, 65–78.

Goddard, J. D. & Miller, C. 1967 Nonlinear effects in the rheology of dilute suspensions. *J. Fluid Mech.* **28**, 657–673.

Hill, R. 1963 Elastic properties of reinforced solids: Some theoretical principles. *J. Mech. Phys. Solids* **11**, 357–372.

Hinch, E. J. 1975 The mechanics of fluid suspensions. In *Theoretical Rheology* (ed. J. F. Hutton, J. R. A. Pearson & K. Walters), pp. 206–223. Wiley.

Hinch, E. J. & Leal, L. G. 1976 Constitutive equations in suspension mechanics. Part 2. Approximate forms for a suspension of rigid particles affected by Brownian rotations. *J. Fluid Mech.* **76**, 187–208.

Howard, I. C. & Brierley, P. 1976 On the finite deformation of an inhomogeneity in a viscous liquid. *Intl J. Engng Sci.* **14**, 1151–1159.

Jeffery, G. B. 1922 The motion of ellipsoidal particles immersed in a viscous fluid. *Proc. R. Soc. Lond.* A **102**, 161–179.

Kalb, B., Cox, R. G. & Manley, R. St. J. 1981 Hydrodynamically induced formation of cellulose fibers II. Fiber formation by deformation of drops with zero interfacial tension. *J. Colloid Interface Sci.* **82**, 286–297.

Kennedy, M. R., Pozrikidis, C. & Skalak, R. 1994 Motion and deformation of liquid drops, and the rheology of dilute emulsions in simple shear flow. *Computers Fluids* **23**, 251–278.

Khakhar, D. V. & Ottino, J. M. 1986 Deformation and breakup of slender drops in linear flows. *J. Fluid Mech.* **166**, 265–285.

Khakhar, D. V. & Ottino, J. M. 1987 Breakup of liquid threads in linear flows. *Intl J. Multiphase Flow* **13**, 71–86.

Levitt, L. & Macosko, C. W. 1996 Influence of normal stress difference on polymer drop deformation. *Polymer Engng Sci.* **36**, 1647–1655.

Maffettone, P. L. & Minale, M. 1998 Equation of change for ellipsoidal drops in viscous flow. *J. Non-Newtonian Fluid Mech.* **78**, 227–241.

Mellema, J. & Willemse, M. W. M. 1983 Effective viscosity of dispersions approached by a statistical continuum method. *Physica* **122A**, 286–312.

Mura, T. 1982 *Micromechanics of Defects in Solids*. Martinus Nijhoff.

Press, W. H., Teukolsky, S. A., Vetterling, W. T. & Flannery, B. P. 1992 *Numerical Recipes in FORTRAN*, 2nd Edn. Cambridge University Press.

Rallison, J. M. 1980 Note on the time-dependent deformation of a viscous drop which is almost spherical. *J. Fluid Mech.* **98**, 625–633.

Roscoe, R. 1967 On the rheology of a suspension of viscoelastic spheres in a viscous liquid. *J. Fluid Mech.* **28**, 273–293.

Rumscheidt, F. D. & Mason, S. G. 1961 Particle motions in sheared suspensions XII. Deformation and burst of fluid drops in shear and hyperbolic flow. *J. Colloid Sci.* **16**, 238–261.

Spence, D. A., Ockendon, J. R., Wilmott, P., Turcotte, D. L. & Kellogg, L. H. 1988 Convective mixing in the mantle: The role of viscosity differences. *Geophys. J.* **95**, 79–86.

Taya, M. & Arsenault, R. J. 1989 *Metal Matrix Composites: Thermomechanical Behaviour*. Pergamon.

Taylor, G. I. 1932 The viscosity of a fluid containing small drops of another fluid. *Proc. R. Soc. Lond.* A **138**, 41–48.

Taylor, G. I. 1934 The formation of emulsions in definable fields of flow. *Proc. R. Soc. Lond.* A **146**, 501–523.

Taylor, G. I. 1964 Conical free surfaces and fluid interfaces. In *Proc. Int. Congr. Appl. Mech., 11th, Munich*, pp. 790–796.

Torza, S., Cox, R. G. & Mason, S. G. 1972 Particle motions in sheared suspensions XXVII. Transient and steady deformation and burst of liquid drops. *J. Colloid Interface Sci.* **38**, 395–411.

Tucker, C. L. & Liang, E. 1999 Stiffness predictions for unidirectional short fiber composites: Review and evaluation. *Compos. Sci. Tech.* **59**, 655–671.

Wetzel, E. 1999 Modeling flow-induced microstructure of inhomogenous liquid-liquid mixtures. PhD thesis, University of Illinois at Urbana-Champaign.

Wilmott, P. 1989*a* The stretching of a slender, axisymmetric, viscous inclusion – Part I: Asymptotic analysis. *SIAM J. Appl. Maths* **49**, 1608–1616.

Wilmott, P. 1989*b* The stretching of a thin viscous inclusion and the drawing of glass sheets. *Phys. Fluids* A **1**, 1098–1103.